Chapter 3

Comparative Study of Conservative and Non-Conservative Interpolation Schemes for the Domain Decomposition Method on Laminar Incompressible Flows

Main contents of this chapter are published as
J. Cadafalch, A. Oliva, C.D. Pérez-Segarra, M. Costa and J. Salom. Comparative study of conservative and nonconservative interpolation schemes for the domain decomposition method on laminar incompressible flow. *Numerical Heat Transfer, Part B*, 35:65-84, 1999.

Abstract. This study examines the resolution of the Navier-Stokes equations for laminar natural or forced incompressible flows by means of the domain decomposition method. Conservative and non-conservative interpolation schemes available in the literature are studied and compared to a formulation completely based on finite-volume techniques. The discretized governing equations are obtained in each subdomain using a finite-volume method on staggered grids and are solved adopting a pressure-based segregated algorithm. A mesh refinement study and the generalized Richardson extrapolation have been adopted to evaluate the errors and the order of accuracy of each interpolation scheme. Illustrative numerical results of a complex flow through a junction are shown.

3.1 Introduction

The resolution of the Navier-Stokes equations applied to incompressible flows is quite a cumbersome problem that appears in many engineering mechanical problems. The scientific community has developed several numerical methods, such as finite-volume or finite-element methods, using structured or unstructured meshes. When fine meshes are used in zones with high gradients, the structured grids force inevitably a fine mesh in the zones with smooth gradients. Moreover, it is quite common in problems with complicated geometry to use rectangular or cylindrical coordinates, approximating the geometry boundaries in a step-wise manner (blocking-off techniques). In all these cases the computer memory and the calculation time are clearly penalized. With *Domain Decomposition Methods* these problems can be avoided, and the codes can be easily parallelized, thus increasing the computational power [1]. In the domain decomposition methods the whole domain is divided into several *Subdomains* joined by the interpolation boundaries. The discretized governing equations are solved in each subdomain with the appropriate boundary conditions and the required grid and numerical scheme. Therefore, the discretized system of equations that defines the physical processes in a problem is divided into smaller systems of equations, each one representative of one subdomain, which can be solved simultaneously by different CPUs. The boundary conditions in the interpolation boundaries are calculated via procedures called *Interpolation Schemes*, which are responsible for the information transfer among subdomains.

Several methods for the domain decomposition have been developed. They can be classified into two large groups: *Patched Grid*, in which the domain is divided into subdomains without overlapping zones [2]; and *Overlapping Grid* which divides the domain into overlapped subdomains [3][4].

Two different interpolation types will be considered in this work:

- Interpolations based on finite-volume techniques. The fluxes through an interpolation boundary (i.e. mass, momentum or heat fluxes) are calculated from local balances in the source subdomain and are introduced as a boundary condition in the sink subdomain. This procedure will be named as *Conservative Interpolation*.

- Mathematical interpolations (such as Lagrange interpolations), which are usually *Non-Conservative.*

Many efforts have recently been carried out for the resolution of the Navier-Stokes equations using domain decomposition methods in incompressible flows. Chesshire and Henshaw [4][5] have studied in great detail the domain decomposition method for the numerical resolution of one 2nd order PDE, such as Burger's equation. They have developed conservative and non-conservative interpolation schemes on overlapping

grids and established criteria for the evaluation of the accuracy of the solution. Zang and Street [6] solved the pressure Poisson equation globally and the velocity in each subdomain using a conservative scheme for the mass balance (MIC). And Shyy et al. [3][7] have used conservative interpolation schemes with the SIMPLE algorithm.

Although in the literature it is widely accepted that conservative schemes for the domain decomposition method on incompressible flows are recommended, there are some problems which have not been resolved yet. They can be briefly described by the following questions:

- Could the conclusions of studies on one 2nd order PDE be directly applied on the Navier-Stokes equations? Otherwise, do these equations require specific interpolation schemes?
- What kind of physical fluxes need to be preserved in order to accomplish the condition of well-posedness?
- Do the errors introduced by the imbalances of the non-conservative interpolations disappear with the mesh refinement?

This work is focussed on the analysis of the above described questions. The studies have been restricted to two-dimensional Cartesian grids that overlap at arbitrary angles in order to carry out the analysis in greater detail. However, the extension of this study and its conclusions to three-dimensional and body fitted coordinates is straightforward. Different interpolation schemes (conservative and non-conservative) already available and used in the literature have been studied and compared together with a fully-conservative formulation completely based on finite-volume techniques. The discretized governing equations are obtained using the finite-volume method. The set of algebraic equations is solved in a segregated manner using the SIMPLEC algorithm [8][9]. The geometry is discretized with structured Cartesian staggered grids, and both high and low-order accurate numerical schemes are adopted for the numerical discretization. The algebraic system of equations has been solved with a multigrid algebraic solver [10] with explicit information transfer between subdomains.

During the last years the computational fluid dynamics community has been pointing out the need of improving the rigor of the numerical results. Many authors have discussed the importance of using high-order numerical schemes [11]. Techniques such as the Grid Convergence Index (GCI) [12] have been developed in order to control the numerical uncertainty. In this work the numerical errors and the order of accuracy of the computational solutions have been estimated using a post processing tool based on the Richardson extrapolation [13]. This tool has given criteria about the uncertainty introduced by the interpolation schemes.

The following section presents the mathematical formulation and an overview of the finite-volume formulation proposed. The finite-volume local balances used in

the conservative interpolation schemes, and the principles of the conservative and non-conservative interpolation schemes are described. Finally, some comments of the mathematics involved in the estimation of errors and order of accuracy of the numerical solutions are given.

In section 3.3, the results of a comparative study of three different interpolation schemes for the velocity field and three different interpolation schemes for the scalar fields (temperature) are presented. The same problems have been solved using an h-refinement criterion (mesh-refinement) on a non-decomposed domain and on a decomposed domain with the studied interpolation schemes. Then, the comparison of the numerical errors and the order of accuracy of the numerical solutions has given criteria about the suitability of the interpolation schemes.

3.2 Formulation

3.2.1 Governing equations

Though a bi-dimensional formulation will be used for convenience, all the equations and results hereafter presented and discussed can be extrapolated to three-dimensional problems. All the thermophysical properties are constant except the influence of density variations in the body term of the momentum equations (Boussinesq approximation).

The set of governing equations can be joined in the convection-diffusion equation:

$$\frac{\partial(\rho\phi)}{\partial t} + \nabla \cdot (\mathbf{j}) = S \tag{3.1}$$

where the total flux $\mathbf{j}$ is made up of the convection flux ($\mathbf{j}^C$) and the diffusion flux ($\mathbf{j}^D$) as follows:

$$\mathbf{j} = \rho\mathbf{v}\phi - \Gamma\nabla\phi = \mathbf{j}^C + \mathbf{j}^D \tag{3.2}$$

and where the dependent variable ϕ, the diffusion coefficient Γ and the source term S depend on the transport equation [8].

The fully-implicit discretized form of the convection-diffusion equation on a finite rectangular-volume of volume V_P is as follows:

$$\rho\frac{\phi_P - \phi_P^\circ}{\Delta t}V_P + J_e - J_w + J_n - J_s = SV_P \tag{3.3}$$

where J_i are the fluxes (mass, momentum or heat fluxes) through the control volume faces. For example, for a west face of area A_y,

$$J_w = \left(\rho u\phi - \Gamma\frac{\partial\phi}{\partial x}\right)_w A_y = J_w^C + J_w^D \tag{3.4}$$

Introducing (3.4) in (3.3) and adopting the numerical scheme, the algebraic discretized equation takes the form [8]:

$$a_P\phi_P = a_E\phi_E + a_W\phi_W + a_N\phi_N + a_S\phi_S + b \tag{3.5}$$

where the algebraic coefficients a_i and b are function of the local Peclet number, the mass flow rates through the cell faces, the diffusive coefficients, the transient term, the source term, the cells' dimensions and the correction term corresponding to the deferred-correction approach [14].

The integral fluxes through the cell faces (3.4) can be calculated in terms of the values involved in the algebraic formulation. For example, for the west face,

$$J_w = a_W\phi_W - (a_W - F_w)\phi_P - F_w(\phi_w^l - \phi_w^h) \tag{3.6}$$

where ϕ_w^l stands for the ϕ value at the west face estimated with the low-order numerical scheme, ϕ_w^h stands for the ϕ value at the west face estimated with the high-order numerical scheme, and F_w is the mass flow through the west face.

3.2.2 Flux through an arbitrary area inside the control volume

For convenience, the explanation will firstly be carried out on the calculation of the flux through an arbitrary section parallel to the control volume faces (Fig. 3.1a). For the control volume $\hat{CV}$ a similar balance to the one carried out in equation (3.3) leads to:

$$\hat{\beta}\rho\frac{\phi_P - \phi_P^\circ}{\Delta t}V_P + \hat{J}_x - J_w + \hat{\alpha}J_n - \hat{\alpha}J_s = \hat{\beta}SV_P \tag{3.7}$$

where $\hat{\beta}$ and $\hat{\alpha}$ are geometric ratios between $\hat{CV}$ and CV ($\hat{\beta} = \hat{V}/V_P$ and $\hat{\alpha} = \hat{A}_x/A_x$).

As $\hat{\beta} = \hat{\alpha}$, manipulating (3.3) and (3.7), $\hat{J}_x$ can be expressed as a linear interpolation of the known fluxes J_w and J_e:

$$\hat{J}_x = J_w + \hat{\beta}(J_e - J_w) \tag{3.8}$$

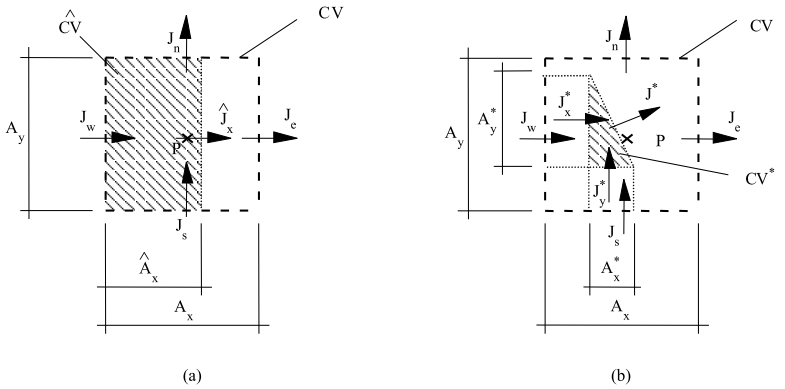

Figure 3.1: Local balance for the calculation of a flux through a section. (a) Section parallel to the control volume faces. (b) General case.

Now, the general case presented in Fig. 3.1b will be discussed. The local balance at the shaded control volume CV^* is

$$\beta^* \rho \frac{\phi_P - \phi_P^\circ}{\Delta t} V_P + J^* - J_x^* - J_y^* = \beta^* S V_P \tag{3.9}$$

where β^* is the volume ratio between CV^* and CV ($\beta^* = V^*/V_P$). Then, introducing equation (3.3) in (3.9), the flux J^* of Fig. 3.1b can be expressed as follows:

$$J^* = J_x^* + J_y^* + \beta^*(J_e - J_w + J_n - J_s) \tag{3.10}$$

where $J_x^* = (A_y^*/A_y)\hat{J}_x$, $J_y^* = (A_x^*/A_x)\hat{J}_y$ and $\hat{J}_x$ and $\hat{J}_y$ can be obtained from linear interpolations of the known fluxes at the cell faces, equation (3.8). As J^* has been obtained via local balances, the global balances are also preserved.

3.2.3 Interpolation Schemes

Description

This explanation will be focussed on the interpolations of a generic variable ϕ_W in the west interpolation face of the sink subdomain control volume shown in Fig. 3.2a.

The boundary conditions in a control volume that belongs to an interpolation boundary have to be calculated from the source subdomain. Fig. 3.2b shows the

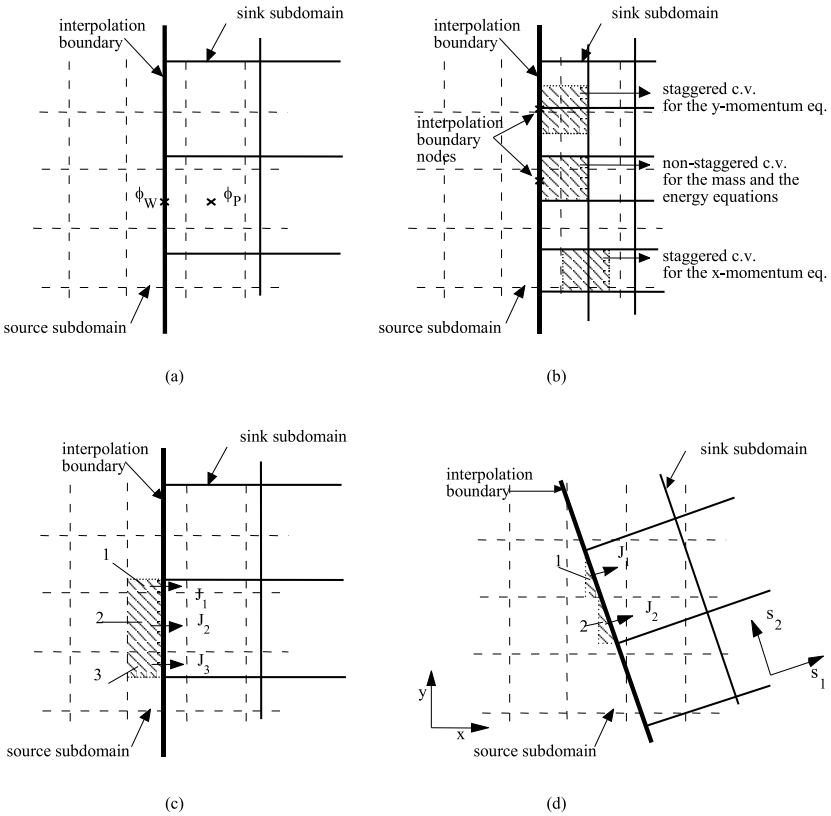

Figure 3.2: Interpolation in a west control volume face. (a) Subdomains with parallel axis. (b) Interpolation boundary nodes for the mass, energy and tangential-momentum equation (non-interpolated information for the entrance-momentum equation is used). (c) Subdomains with parallel axis. Local balance. (d) Sloped subdomains. Local balance.

interpolation boundary nodes involved in a west interpolation boundary. Boundary conditions have been given for the mass, energy and y-momentum equations (i.e. entrance velocity, temperature and tangential velocity at the boundary node for Dirichlet boundary conditions, and mass, heat and tangential-momentum fluxes for Neumann conditions). In simply-connected flow domains the entrance momentum boundary condition is not needed, however in multiply-connected flow domains this boundary condition is necessary to avoid unrealistic solutions [15]. The interpolation procedure for all the variables are analogous, using the appropriate meshes in both sink and source subdomains.

Non-conservative interpolation schemes. A bi-dimensional Lagrange interpolation is adopted. According to Chesshire and Henshaw [4], the order of accuracy of an interpolation scheme has to be at least one order higher than that of the numerical discretization to preserve the overall accuracy. All the nonconservative interpolations considered here are bi-quadratic interpolations, which are third-order accurate. With this kind of interpolation, the conservation of physical fluxes through the interpolation face is not guaranteed because no balances are made.

Conservative interpolation schemes. The flux (mass, tangential-momentum or energy flux) through the interpolation boundary is calculated from a local balance (see section 3.2.2), and it is introduced as a boundary condition of the sink subdomain. Then, the conservative boundary condition for the mass, the tangential-momentum and the energy equation of the sink subdomain, are obtained by a mass, tangential-momentum and heat local balance at the source subdomain.

Thus, the flux J_w through the west interpolation face presented in Fig. 3.2c is

$$J_w = J_1 + J_2 + J_3 \tag{3.11}$$

where J_1, J_2 and J_3 are calculated from local balances on the shaded control volumes. J_w can be introduced directly as a boundary condition in the sink grid reformulating the algebraic coefficients, see [3], or as a boundary value ϕ_W in such a way that the prescribed flux is automatically satisfied in the sink control volume. That is, using the flux equation (3.6) as follows,

$$\phi_W = \frac{J_w + (a_W - F_w)\phi_P}{a_W} \tag{3.12}$$

where the internal nodal value ϕ_P is treated in an explicit manner for convenience. It is worth mentioning that at the boundaries the deferred-corrective convection term is equal to zero, and thus, it has not been considered in equation (3.12).

Interpolation schemes on sloped subdomains

The previous description has been focused on the information exchange between two subdomains with parallel axis (Fig. 3.2a). Its generalization to sloped subdomains involves some aspects that will now be discussed on the control volume face depicted in Fig. 3.2d.

Interpolation of scalar variables (temperature). The treatment of scalar variables does not introduce any modification either for the formulation of the Lagrange interpolations or for the formulation of the conservative schemes, keeping in mind that now the local balance to be carried out is the one depicted in Fig. 3.2d.

Interpolation of the velocity field. When a velocity component of an interpolation boundary is interpolated from the velocity field of a source subdomain with parallel axis, only the field of the velocity component in the studied direction is required. Thus, the velocity field can be interpolated as two segregated scalar fields (in bi-dimensional problems). However, when sloped subdomains are involved, the velocity field has to be considered as a vector field. In order to interpolate a velocity component with a bi-dimensional Lagrange interpolation, it is necessary to interpolate the velocity vector (from the source subdomain information) and project it into the desired direction of the coordinate system of the sink subdomain (s_1 or s_2 directions).

Concerning the conservative interpolation of the velocity field, two kinds of fluxes have to be taken into account: the mass and the tangential-momentum flux through the sink subdomain interpolation boundary. The required balances (mass balance and momentum balance in the s_2 direction, see Fig. 3.2d), have to be studied in a different way.

The mass flux going through the depicted west face in Fig. 3.2d is obtained via

$$J_w = J_1 + J_2 \tag{3.13}$$

where J_1 and J_2 are calculated from local mass balances on the shaded control volumes 1 and 2 of the source subdomain and J_w stands for the mass flux through the studied face.

On the other hand, a momentum balance implies the manipulation of the vector momentum equation. For convenience, in the discretized formulation this vector equation is decomposed into one equation for each direction (the x-momentum and y-momentum equations for the source subdomain, and the s_1-momentum and s_2-momentum equations for the sink subdomain). Hence, considering the west boundary face of Fig. 3.2d as a section of the source subdomain, it is crossed by two kinds of momentum fluxes: the x-momentum flux and the y-momentum flux. That gives the momentum flux a vector profile:

$$\mathbf{J}_{mom} = (J_{x-mom}, J_{y-mom}) \tag{3.14}$$

Therefore, the momentum flux in the tangential direction (s_2-momentum flux) can be easily obtained from the projection of the momentum flux vector in the s_2 direction. This procedure requires two balances of the same kind of equation (3.13) for the calculation of J_{x-mom} and J_{y-mom}. The former has to be carried out using the x -staggered mesh of the source subdomain and the latter using the y-staggered mesh. It can be seen that when the subdomains have parallel axis ($\{\mathbf{x}, \mathbf{y}\} = \{\mathbf{s}_1, \mathbf{s}_2\}$), the entrance component of the vector momentum flux is not needed. Then the conservative boundary condition for the tangential-momentum equation is obtained only from the information of the source momentum equation in the tangential direction (as explained in section 3.2.3).

3.2.4 Errors and order of accuracy of a numerical solution

General aspects

In numerical heat transfer and computational fluid dynamics the computational errors are due to the discretization errors when the convergence criteria is strong enough. There are two discretization error sources: the geometric discretization (mesh size), and the numerical schemes. In order to quantify each of them two different parameters are usually adopted:
h: geometric discretization parameter (representative of the mesh spacing). p: order of accuracy of the numerical schemes.

The local discretization error (at an $\mathbf{x}$ point of the domain) in a numerical solution can be expressed as [13]

$$e_D(\mathbf{x}) = C_p(\mathbf{x})h^p \tag{3.15}$$

where $C_p(\mathbf{x})$ depends on the numerical scheme. If the refinement level is strong enough the solution belongs to the called asymptotic range. In this range the error can be estimated, and so, the uncertainty of the numerical solution can be controlled.

The h-refinement treatment is commonly used to reduce the discretization errors. A numerical scheme is fixed and h is refined. In h-refinement studies, the Richardson extrapolation has usually been adopted as a formally upper-order extrapolated solution estimator and as an error estimator [12]. Accordingly, two solutions of the problem in the asymptotic range are required. This theory can also be used as a p estimator [13]. With three solutions of a problem (ϕ_1, ϕ_2 and ϕ_3) obtained on the grids $h_1 = h$ (fine grid), $h_2 = rh$ (middle grid) and $h_3 = r^2h$ (coarse grid), a three

equation system of the unknown variables p, ϕ_E (extrapolated solution) and $C_p(\mathbf{x})$ can be posed:

$$e_{Di} = \phi_i - \phi_E = C_p(\mathbf{x})(r^{i-1}h)^p \qquad i = 1, 2, 3 \tag{3.16}$$

from which it can be determined that

$$p = \frac{ln[(\phi_2 - \phi_3)/(\phi_1 - \phi_2)]}{lnr} \tag{3.17}$$

This equation must be used with caution, because the Richardson extrapolation involves the assumptions of smoothness and monotone error convergence in the mesh spacing h.

Evaluation of the error of a numerical solution

In order to calculate the error of a numerical solution, it would be necessary to know the exact solution of the governing equations. Usually, the exact solution is unknown, and a grid independent numerical solution is taken as a reference or "exact" solution. Some grid-independent benchmark solutions are given in the literature. They give information of global values (such as the average Nu or the velocity distribution in a section of the domain), which are useful for the code validation, but are limited for a detailed error evaluation. Thus, a grid independent solution has been calculated for all the testing problems used in this paper. They have been considered the "exact" or reference solution for the error studies. Then, the numerical normalized error maps of the same testing problems solved on different grids, domain decompositions or numerical schemes have been carried out by

$$e^*_D(\mathbf{x}) = \mid \phi^*(\mathbf{x}) - \phi^*_E(\mathbf{x}) \mid \tag{3.18}$$

where $\phi^*(\mathbf{x})$ is the normalized solution, $\phi^*_E(\mathbf{x})$ is the normalized "exact" solution and $\mathbf{x}$ stands for the coordinates of the discretization nodes of the studied solution (position vector). These nodal coordinates of the studied cases generally do not coincide with the nodal coordinates of the "exact" solution. Then an interpolation of the exact solution nodal values is needed. This is an important aspect in this analysis. If a low-order accurate interpolation is used, the obtained error map is not representative of the real solution error. Bi-quadratic interpolations (3rd order accurate) have been used. The average of the local error has been adopted as a global error estimator.

Evaluation of the order of accuracy of a numerical solution

Generally, it is not possible to know the order of accuracy of a solution a priori. It depends on the accuracy of the numerical schemes used in the inner and boundary diffusive and convective terms. The calculated terms accuracy in some cases is formally known (when the numerical scheme is, for example, upwind or central difference), but when hybrid schemes like power-law are used, the order of accuracy is bounded but not fixed (it depends on the nature of the problem). Furthermore, different accurate schemes are usually adopted in the calculation of the diffusive and convective terms. The more and less accurate scheme in a problem bound the expected values of p. This can be used as a post-processing tool to ensure the certainty of a numerical solution.

With three different solutions obtained from an h-refinement study with a refinement ratio r, equation (3.17) allows the estimation of local and global p values (if local values or global values are processed).

In the local studies, generally the nodal coordinates of the calculated solution do not coincide. The analysis here presented has been carried out at the coarse mesh nodes, using bi-quadratic interpolations of the finer grid values.

When a calculated p is out of the expected bounds, this is an indicator that the Richardson extrapolation cannot be applied. There are two possible causes: ϕ values are nearly zero, or the studied solution values do not belong to the asymptotic range and, thus, a finer mesh is required. Furthermore, in some problems, or in some zones of the studied domain, where the solution converges in an oscillatory way when h is refined, the Richardson extrapolation has no meaning. In the local studies of p presented in this work, p has been calculated in all the nodes using equation (3.17) except in the oscillatory nodes and the nodes with ϕ near zero, and the average p has been taken as a representative value of the global p distribution.

3.3 Results

3.3.1 Comparative study of the interpolation schemes

Description

The numerical error and the order of accuracy have been chosen as the criteria to analyze the interpolation schemes. For different numerical schemes (i.e. upwind (UDS), central difference (CDS) and SMART [16]) the testing problems have been solved without domain decomposition (on nxn square control volumes) and with domain decomposition with the studied interpolation scheme. The evolution of the numerical errors and the order of accuracy of both solutions when the mesh is refined (with and h-refinement of $r = 2$ and five refinement levels: $n = 10$, $n = 20$, $n = 40$, $n = 80$ and $n = 160$) have been compared. All the differences that have been detected

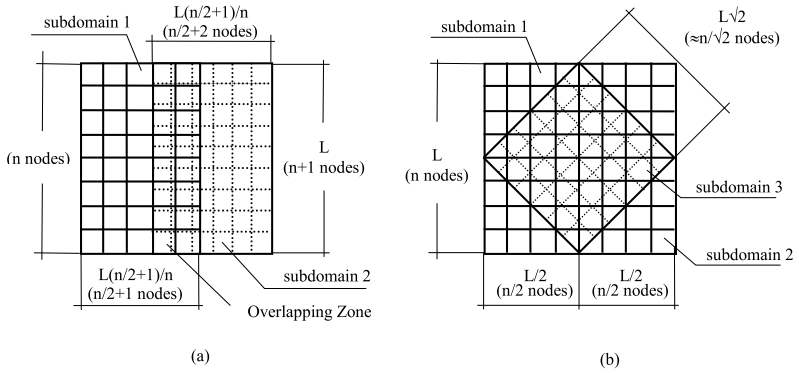

Figure 3.3: Domain decomposition for a square cavity of length L. (a) Two non-sloped subdomains. (b) Three sloped subdomains.

are due to the interpolation scheme. This analysis has been carried out for all the dependent variables. As similar results have been obtained for all of them, only the corresponding ones to the u-field are given.

Three studies (I, II and III) are presented. Study I and II analyze the behavior of different conservative and non-conservative interpolation schemes for the velocity and the scalar field (temperature) in the domain decomposition represented in Fig. 3.3a (non-coinciding meshes in the overlapping zone are used, otherwise the mass flux is automatically preserved for all the studied interpolation schemes [17]). The conclusions of studies I and II are checked in study III on a more complex domain decomposition involving sloped subdomains (Fig. 3.3b).

These studies have been carried out on two testing problems hereafter called A and B. Problem A is a square cavity whose topside moves with a uniform velocity in its own plain (forced convection) with $Re = 10^2$; and problem B is a square cavity with top and bottom adiabatic sides and differentially heated vertical sides (natural convection) with $Ra = 10^5$ and $Pr = 0.71$.

The required grid independent solutions for the evaluation of the error evolution (see section 3.2.4), have been obtained on a $160x160$ uniform grid using SMART . The u-field values in problem A (forced convection) have been normalized by the u-maximum value (i.e. velocity of the moving wall), and in problem B by a reference velocity of $u_\infty = k/\rho c_p L$.

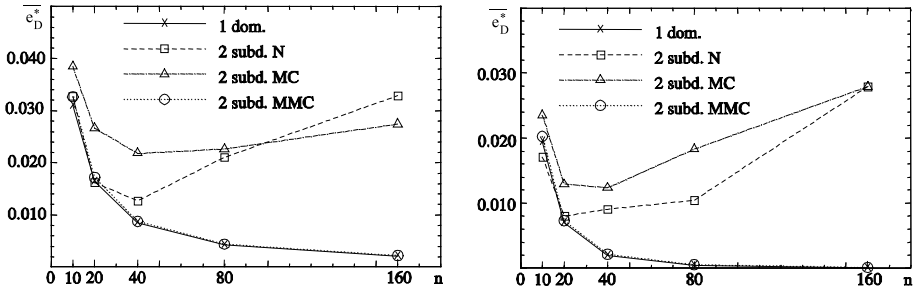

Figure 3.4: Average absolute normalized error of the u-field vs. discretization level in problem A using UDS and CDS.

Study I: Interpolation of the velocity field

The mass and tangential-momentum conservation has been studied in problem A (forced convection). Three different interpolation schemes have been adopted to couple the subdomains:

- N (No-conservation): bi-quadratic interpolation for both entrance and tangential velocities.
- MC (Mass Conservation): conservative interpolation for the entrance velocity (mass balance) and bi-quadratic non-conservative interpolation for the tangential velocity.
- MMC (Mass and Momentum Conservation): conservative interpolation for both entrance and tangential velocity (mass and momentum balances).

Fig. 3.4 Table 3.1 have been obtained solving problem A by means of UDS and CDS. The study has been carried out both on one domain and on the decomposed domain shown in Fig. 3.3a with the interpolation schemes N, MC and MMC. Fig. 3.4 shows the average absolute normalized error of the u variable when the mesh is refined. Table 3.1 shows the average values of p calculated from the u-field maps. For example, observing the results employing UDS, with the set of the coarsest solutions (n=10, 20 and 40) the average p for the non-decomposed domain solution (1 dom.) is 1.12, and for the decomposed domain solutions are: .23 when the domains are coupled by N, 1.47 when they are coupled by MC and .91 when they are coupled by MMC. The average p when the meshes are refined for both the one domain solution and the

	$\bar{p}$							
grid	UDS				CDS			
		2 subd	2 subd	2 subd		2 subd	2 subd	2 subd
$n_3/n_2/n_1$	1 dom	N	MC	MMC	1 dom	N	MC	MMC
10/20/40	1.12	0.23	1.47	0.91	1.30	0.60	1.16	1.25
20/40/80	0.94	-0.07	0.30	0.90	1.78	0.93	-1.07	1.77
40/80/160	1.01	0.01	-0.52	0.99	1.98	-2.25	-0.38	1.88

Table 3.1: Average p of the u-field in problem A using UDS and CDS.

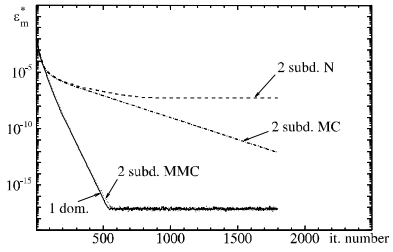

Figure 3.5: Evolution of the normalized mass error with the number of iterations (problem A using UDS and n=40).

solution using MMC, are near 1 (1.01 and .99 respectively), which is the expected order of accuracy corresponding to the UDS numerical scheme. On the other hand, the average p coupling the subdomains using N or MC have meaningless values.

When mass and tangential momentum fluxes through the interpolation faces are preserved, the numerical error introduced by the interpolation scheme is not significant and it disappears when the mesh is refined. Furthermore, p achieves the expected values. On the other hand, if any non-conservative interpolation is adopted to calculate the tangential or entrance velocity, a numerical error due to the interpolation is generated and does not improve when the mesh is refined, and the order of accuracy, p, for these cases has meaningless values.

In addition, MMC has the lower computational cost since the imbalances introduced by non-conservative interpolations make the convergence difficult. In Fig. 3.5 the evolution of the normalized mass error (ϵ_m^*) with the iteration number is given using UDS and n=40. In this particular case the domain decomposed solution using MMC and the one domain solution require the same number of iterations. At the very

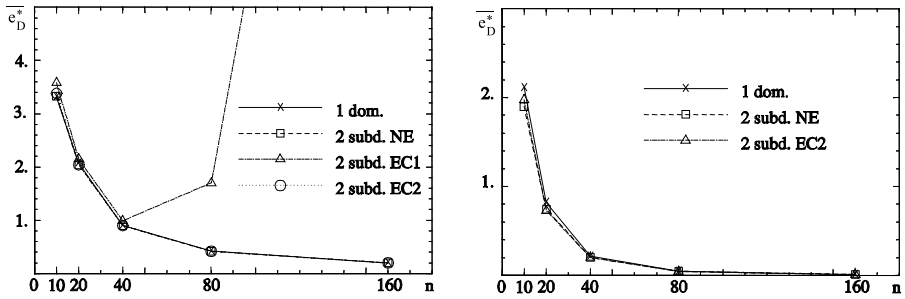

Figure 3.6: Average absolute normalized error of the u-field vs. discretization level in problem B using UDS and CDS.

beginning of the number of iterations all the curves (i.e. 1 dom., N, MC and MMC) coincide. In this zone, as the numerical solution is still far from the asymptotic solution the imbalances introduced by N and MC do not affect the convergence. However, after approximately 100 iterations, the convergence becomes slower for these schemes. Furthermore, as N does not preserve the conservation of mass, with this scheme the normalized mass error cannot be reduced beyond 10^{-7}. This convergence difficulty for N and MC compared to MMC has found to be a general tendency that has been observed in all the studies.

Study II: Interpolation of scalar fields (temperature)

Problem B (natural convection) has been adopted to study the behavior of the scalar fields (in this case the temperature). For the velocity field the best of the analyzed schemes (conservation of mass and momentum) has been adopted. Three different schemes for the temperature interpolation have been studied:

- NE (No-Energy conservation): bi-quadratic interpolation.
- EC1 (Energy Conservation 1): conservative interpolation (heat balances).
- EC2 (Energy Conservation 2): conservative interpolation based on heat balances in one subdomain and on bi-quadratic interpolations in the other (mixed scheme).

Fig. 3.6 and Table 3.2 show the average errors and the order of accuracy obtained solving problem B on one domain and on the decomposed domain shown in Fig. 3.3a

	$\bar{p}$						
grid	UDS				CDS		
		2 subd	2 subd	2 subd		2 subd	2 subd
$n_3/n_2/n_1$	1 dom	NE	EC1	EC2	1 dom	NE	EC2
10/20/40	-0.08	-0.21	-0.13	-0.15	1.18	0.91	1.09
20/40/80	1.35	1.26	-0.56	1.27	1.79	1.73	1.73
40/80/160	1.32	1.27	-1.86	1.30	1.97	1.97	1.89

Table 3.2: Average p of the u-field in problem B using UDS and CDS.

with the studied interpolation schemes NE, EC1 and EC2. The numerical schemes UDS and CDS have been adopted. The results with both NE and EC2 schemes agree with the values calculated with the non-decomposed domain solution. However, the values estimated for the interpolation scheme based only on flux balances (EC1) have no meaning. These values are only given for the study with UDS.

The conservative scheme EC1 is not proper because this scheme makes the set of discretization equations indeterminate. As a consequence, an unphysical jump in the numerical solution of the scalar variable appears in the interpolation boundary [18][19].

The NE and EC2 interpolation schemes have been found as appropriate schemes for the interpolation of scalar fields. Non-important differences in the computational cost have been detected in the tested cases, and the asymptotic numerical solution when the mesh is refined is the same. In Fig. 3.7a the evolution of the normalized mass error (ϵ_m^*) with the iteration number is given using UDS and n=40. The coincidence of the curves corresponding to NE and EC2 can be observed. In this specific study, the use of domain decomposition with explicit information transfer increases the number of iterations required compared to the one domain solution for all the studied interpolation schemes.

The imbalances introduced by NE in the previous studies have been analyzed comparing the average Nu in the west and east boundary faces of the square cavity. As expected, the imbalance is reduced with the mesh refinement. In this case the flux balances are not relevant due to the low values of the velocities and gradients. Even for the coarse mesh (n=10) the discrepancies are less than 0.2% . In other studies not presented here more important imbalance has been detected.

Some mathematical aspects about the interpolation schemes for scalar fields The conclusions of the suitability of the interpolation schemes adopted for the scalar fields can be corroborated with a mathematical discussion of a simple problem: the convection-diffusion equation for a steady one-dimensional problem without source

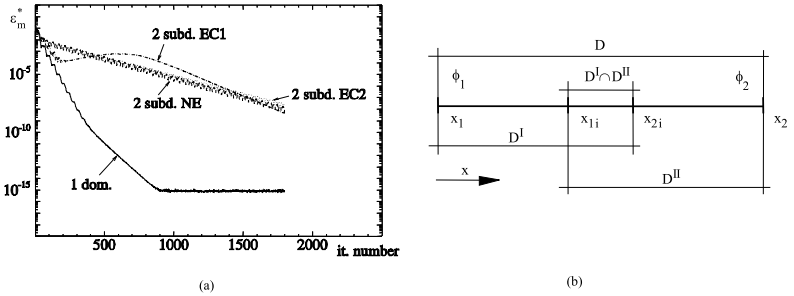

Figure 3.7: (a) Evolution of the normalized mass error with the number of iterations (problem B using UDS and n=40). (b) Physical domain and domain decomposition for the simplified convection-diffusion problem.

term and constant physical properties. The corresponding governing equation is

$$P\frac{\partial \phi}{\partial x} - \frac{\partial^2 \phi}{\partial x^2} = 0 \tag{3.19}$$

where $P = \rho u/\Gamma$. Its analytical solution on the domain $D = [x_1, x_2]$ (Fig. 3.7b) for the Dirichlet boundary conditions $\phi(x_1) = \phi_1$ and $\phi(x_2) = \phi_2$ is as follows:

$$\phi(x) = \frac{\phi_1 - \phi_2}{e^{Px_1} - e^{Px_2}} e^{Px} - \frac{\phi_1 e^{Px_2} - \phi_2 e^{Px_1}}{e^{Px_1} - e^{Px_2}} \tag{3.20}$$

Now, the domain $D = [x_1, x_2]$ will be decomposed into two overlapping subdomains $D^I = [x_1, x_{2i}]$ and $D^{II} = [x_{1i}, x_2]$ where $D^I \cap D^{II} = [x_{1i}, x_{2i}]$ (Fig. 3.7b), and the same problem will be solved analytically coupling the subdomains with the interpolation schemes for scalar variables adopted in the numerical studies: NE, EC1 and EC2.

The differential equation (19) has to be solved twice: in subdomain D^I and in subdomain D^{II}:

$$\phi^I(x) = C_1^I e^{Px} + C_2^I \quad \forall x \in [x_1, x_{2i}] \quad \phi^{II}(x) = C_1^{II} e^{Px} + C_2^{II} \quad \forall x \in [x_{1i}, x_2] \tag{3.21}$$

Four interpolation constants appear, two for every subdomain. Thus, four constrains are required. Two of them are the same boundary conditions used before,

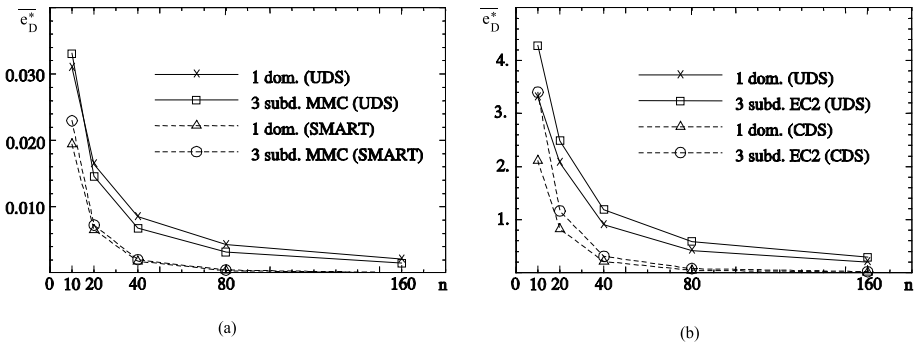

Figure 3.8: Average absolute normalized error of the u-field vs. discretization level. (a) Problem A using UDS and SMART. (b) Problem B using UDS and CDS.

$\phi^I(x_1) = \phi_1$ and $\phi^{II}(x_2) = \phi_2$. The other constrains will be fixed by the interpolation scheme in the two interpolation boundaries ($x = x_{1i}$ and $x = x_{2i}$). A Lagrange interpolation forces the ϕ value to be equal for both subdomains ($\phi^I = \phi^{II}$), and a conservative interpolation scheme forces the equality of fluxes in the interpolation boundary ($J^I = J^{II}$), where the fluxes are evaluated by means of equation (4).

The interpolation constrains, both for the non-conservative scheme (NE) and the mixed scheme (EC2), together with the boundary conditions, give the equation system the desirable solution:

$$\phi^I(x) = \phi(x) \qquad \forall x \in [x_1, x_{2i}] \qquad \phi^{II}(x) = \phi(x) \qquad \forall x \in [x_{1i}, x_2] \qquad (3.22)$$

where $\phi(x)$ is the analytical solution of the problem on a non-decomposed domain, equation (20). However, the two equations corresponding to the interpolation constrains for the fully conservative scheme (EC1) degenerate into only one equation. Thus, only three independent equations are available for the determination of the four integration constants, and it makes the solution of the decomposed domain problem indeterminate.

Study III: Application on sloped subdomains

In studies I and II, only parallel subdomains have been adopted. In order to corroborate the suitability of the mass and tangential-momentum conservative interpolation scheme for the velocity field (MMC), and the no-energy conservative and mixed conservative schemes for the temperature (NE and EC2), different studies on more complicated domain decompositions involving sloped subdomains have been carried

	$\bar{p}$							
	Problem A				Problem B			
grid	UDS		SMART		UDS		CDS	
$n_3/n_2/n_1$	1 dom	3 subd	1 dom	3 subd	1 dom	3 subd	1 dom	3 subd
10/20/40	1.12	1.73	1.51	1.86	-0.08	0.39	1.28	1.57
20/40/80	0.94	1.24	1.97	1.88	1.35	1.24	1.79	1.87
40/80/160	1.01	1.03	2.03	1.79	1.32	1.24	1.97	2.03

Table 3.3: Average p of the u-field in problem A and in problem B for different numerical schemes.

out. Good agreement between the error and p evolution of the non-decomposed domain studies and the decomposed domain studies has always been achieved. Two of these studies are presented in Table 3.3 and in Fig. 3.8. The first is problem A solved using UDS and SMART. The values for the non-decomposed domain solution are compared to the values of the numerical solutions obtained on the domain decomposition exposed in Fig. 3.3b with the MMC scheme. A similar study on problem B is presented adopting the UDS and CDS numerical schemes, and with the EC2 interpolation scheme for the coupling of the subdomains.

It is worth mentioning that in these studies the agreement between the results for non-decomposed and decomposed domain studies is not as good as in the previous studies. The parameter n has been used to characterize the grid density. Thus, the comparison between two solutions in a level n assumes that the level of geometric discretization in both solutions is equal and this has not been exactly kept in this study. As a result, certain discordance is introduced.

3.3.2 Flow in a junction

In section 3.3.1 the suitability of the fully-conservative finite-volume formulation for the domain decomposition method has been proved and compared to the behavior of different non-conservative formulations. Now, the well-posedness of these formulation is checked on a bi-dimensional flow in a junction with two inlets and one outlet (see Fig. 3.9a). A constant entrance velocity profile is given in the inlets ($Re = 10^3$), and in the outlet developed flow conditions are assumed. This problem has been solved on a non-decomposed square domain of size L using the blocking-off technique (approximation of the geometry in a step-wise manner) and on the decomposed domain shown in Fig. 3.9a. A mesh refinement of r=2 and five regular meshes of $n = 10$, $n = 20$, $n = 40$, $n = 80$ and $n = 160$ (where $\Delta x \approx \Delta y \approx 2L/5n$) are used. The grid independent solution in a single blocked-off domain with a grid of 800x800 control

	$\bar{p}$			
grid	UDS		SMART	
$n_3/n_2/n_1$	1 dom	4 subd	1 dom	4 subd
10/20/40	1.12	1.73	1.51	1.86
20/40/80	0.94	1.24	1.97	1.88
40/80/160	1.01	1.03	2.03	1.79

Table 3.4: Average p of the u-field in the junction problem using UDS and SMART.

volumes ($\Delta x = \Delta y = L/800$) and SMART scheme has been considered the reference solution. The numerical errors and the order of accuracy of the numerical solutions using both UDS and SMART schemes are presented in Fig. 3.9b and Table 3.4, where the u-component of the velocity has been normalized respect to the entrance velocity. Good agreement between the results in the non-decomposed domain and in the decomposed domain is achieved, and expected values for the order of accuracy are obtained. The discordance, especially in the average order of accuracy p, is more important than in the previous studies. With the adopted domain decomposition most control volumes are orientated in the flow direction; on the other hand, in the non-decomposed domain the control volumes in the sloped channel are not orientated in the mean flow direction. Thus, the upwind criteria fit better in the decomposed domain, and as a consequence, the order of accuracy of the numerical solutions, especially for coarse grids, may have some differences. Some more discrepancies could arise from the fact that in order to exactly fit the physical geometry the size of the control volumes in both studies has not been kept exactly equal, while the comparison between levels of refinement involves the hypothesis of equality of the grid spacing.

The streamlines of the flow are presented in Fig. 3.9c, and the velocity profiles in sections of the central zone are shown in Fig. 3.9d. In both figures the results are obtained from the finest grid ($\Delta x \approx \Delta y \approx L/400$) using the SMART scheme and the decomposed domain. The developed flow boundary condition at the outlet produces a recirculation in the outer zone. Internal recirculations are detected in the entrance as a consequence of the impinge of the inlet fluxes, and in corners. A small eddy appears at the top corner of the sloped duct, and larger eddies are formed close to the east wall of the sloped duct and at the bottom of the outer duct.

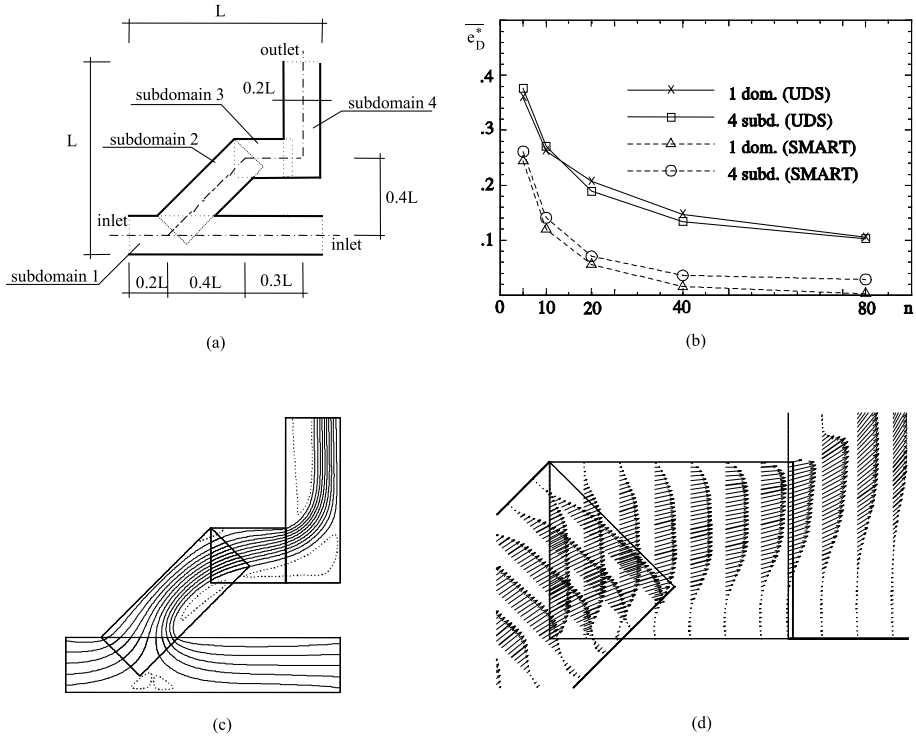

Figure 3.9: Flow in a junction. (a) Physical domain and domain decomposition. (b) Average absolute normalized error of the u-field vs. discretization level using UDS and SMART. (c) Streamlines. Results for the finest mesh ($\Delta x \approx \Delta y \approx L/400$) using the SMART scheme and the decomposed domain. (Solid lines: uniform streamline intervals; dotted lines: non-uniform streamline intervals). (d) Zoom of velocity profiles in the central zone. Results for the finest mesh ($\Delta x \approx \Delta y \approx L/400$) using the SMART scheme and the decomposed domain.

3.4 Conclusions

An essential aspect in domain decomposition methods is the behavior of the interpolation schemes used to relate the physical variables in each domain. Conservative and non-conservative numerical schemes for the Navier-Stokes equations have been studied in detail and compared, together with a well-posed generic conservative domain decomposition formulation completely based on finite-volume techniques. The mass, tangential momentum and energy fluxes through the interpolation boundaries are calculated from local balances in the source subdomain and are introduced as boundary conditions in the sink subdomain.

The numerical errors that the interpolation schemes introduce in the numerical solution have been analyzed, and the Richardson extrapolation has been adopted as a tool to estimate the order of accuracy of the numerical solutions.

From the numerical studies presented here, the suitability of the interpolation scheme for the velocity field based on the conservation of mass and the tangential-momentum flux has been clearly proved. Although in problems with low gradients a non-conservative interpolation scheme for the velocity field might not introduce significant numerical errors, the well-posedness condition is not satisfied, and the imbalances introduced make the method convergence difficult.

For the scalar variables, two schemes have been found suitable: a non-conservative scheme based on Lagrange interpolations, and a conservative scheme based on flux balances in one subdomain and Lagrange interpolations in the other. Although they have similar computational cost, the former introduces imbalances of the physical property (e.g. energy) that for coarse meshes could be important.

3.5 Acknowledgments

This work has been financially supported by the Comisión Interministerial de Ciencia y Tecnología, Spain (project number TIC724-96) and by the Comissionat per Universitats i Recerca de la Generalitat de Catalunya.

Nomenclature

c_p	specific heat	*Greek symbols*	
e_D	discretization error		
g	gravitational acceleration	β	thermal expansion
h	mesh spacing	Δt	interval of time
k	thermal conductivity	μ	dynamic viscosity
L	reference length	ρ	density
n	parameter that defines	ε_m	mass error
	the number of grid nodes	ϕ	generic dependent variable
p	order of numerical accuracy		
p_d	dynamic pressure		
Pr	Prandtl number	*Superscripts*	
r	refinement ratio ($r > 1$)		
Ra	Rayleigh number	e,w,n,s	value at cell face
Re	Reynolds number	P,E,W,N,S	value at cell nodes
T	temperature	∞	reference value
u,v	Cartesian velocities		
	components		
V	volume of a cell	*Subscripts*	
x,y	Cartesian coordinates		
		$*$	normalized value
		$\circ$	value at the previous Δt
		$-$	averaged value

References

[1] D. Drikakis, E. Schreck, and F. Durst. Performance analysis of viscous flow computations on various parallel architectures. *Journal of Fluids Engineering*, 116:635–841, 1994.

[2] D. Lee and J.J. Chiu. Computation of physiological bifurcation flows using a patched grid. *Computers Fluid*, 21(4):519–535, 1992.

[3] J. Wright and W. Shyy. A pressure-based composite grid method for the navier-stokes equations. *Journal of Computational Physics*, 107:225–238, 1993.

[4] G. Chesshire and W.D. Henshaw. Composite overlapping meshes for the solution of partial differential equations. *Journal of Computational Physics*, 90(1):0–0, 1990.

[5] G. Chesshire and W.D. Henshaw. A scheme for conservative interpolation on overlapping grids. *SIAM Journal of Scientific Computing*, 15(4):819–845, 1994.

[6] Y. Zang and R.L. Street. A composite multigrid method for calculating unsteady incompressible flows in geometrically complex domains. *International Journal for Numerical Methods in Fluids*, 20(5):341–361, 1995.

[7] W. Shyy, J. Liu, and J. Wright. Pressure-based visous flow computation using multiblock overlapped curvilinear grids. *Numerical Heat Transfer, Part B*, 25:39–59, 1994.

[8] S.V. Patankar. *Numerical heat transfer and fluid flow.* Hemiosphere Publishing Corporation, 1980.

[9] J.P. Van Doormal and G.D. Raithby. Enhancements of the simple method for predicting incompressible fluid flows. *Numerical Heat Transfer*, 7:147–163, 1984.

[10] B.R. Hutchinson and G.D.Raithby. A multigrid method based on the additive correction strategy. *Numerical Heat Transfer, Part B*, 9:511–537, 1986.

[11] P.J. Roache. Response to the comments by drs. shyy and sindir. *Journal of Fluids Engineering*, 116:198–199, 1996.

[12] P.J. Roache. Perspective: a method for uniform reporting of grid refinement studies. *Journal of Fluids Engineering*, 116:405–413, 1994.

[13] I. Celik and Vei-Ming Zhang. Calculation of numerical uncertainty using richardson extrapolation: application to some simple turbulent flow calculations. *Journal of Fluids Engineering*, 117:439–445, 1995.

[14] P.K. Khosla and S.G. Rubin. A diagonally dominant second-order accurate implicit scheme. *Computational Fluids*, 2:207–209, 1974.

[15] J.A. Wright. *A pressure-based composite grid method for complex fluid flows.* PhD thesis, University of Florida, 1993.

[16] P.H. Gaskell et al. Comparison of two solution strategies for use with higher-order discretization schemes in fluid flow simulation. *International Journal for Numerical Methods in Fluids*, 8:1203–1215, 1988.

[17] J. Salom, J. Cadafalch, A. Oliva, and M. Costa. A subdomain methods in three-dimensional natural and mixed convection in internal flows. In *Proceedings of the IMACS-COST Conference Computational Fluid Dynamics in Three-Dimensional Complex Flows*, pages 289–295, 1995.

[18] J. Wright and W Shyy. Numerical simulation of unsteady convective intrusions in a thermohaline stratification. *International Journal of Heat and Mass Transfer*, 39(6):1183–1201, 1996.

[19] J. Cadafalch, J. Salom, M. Costa, and A. Oliva. Domain decomposition as a method for the parallel computing of laminar incompressible flows. In *Proceedings of the Second European Congress on Computational Methods in Applied Sciences and Engineering (ECCOMAS)*, pages 845–851, 1996.